*"Physics of Auroral Phenomena", Proc. XLII Annual Seminar, Apatity, pp. 57-60, 2019*


Polar Geophysical Institute

DOI: 10.25702/KSC.2588-0039.2019.42.57-60

# ON THE CORRELATION BETWEEN LUNAR CRUSTAL MAGNETIC FIELDS AND THE SOLAR WIND ION REFLECTION MAP

R. Belyaev[1], A. Divin[1], V. Semenov[1], I. Kubyshkin[1], I. Zaytsev[1], J. Deca[2,3]

[1]*Physics Department, St. Petersburg State University, St. Petersburg, Russia*
[2]*Laboratory for Atmospheric and Space Physics, University of Colorado Boulder, Boulder, CO 80303, USA*
[3]*Institute for Modeling Plasma, Atmospheres and Cosmic Dust, NASA/SSERVI, Moffett Field, CA 94035, USA*

**Abstract.** The Moon does not have a global magnetic field. However, the lunar crust contains regions of remanent magnetization which are strong enough to deflect and reflect a substantial part of the incoming solar wind ions. Such effects as lunar swirls, limb shocks, minimagnetospheres, low-frequency waves are the global processes induced by the local magnetic fields. In this work we investigate the correlation between local magnetic field data provided by the Tsunakawa model [2015], and the total particle reflection function estimated by *Lue et al.* [2011]. We find a spatial correlation coefficient between those two up to ~0.7 for the magnetic field model value at 20 km. It was found that an increase in the field leads to a significant increase in reflection and this dependence of the field on the reflection coefficient has a clear nonlinear form, which is consistent with numerical simulation results that show more intense scattering for stronger magnetic anomalies. For low magnetic field regions (<30 nT), the value of reflection coefficient is ~$10^{-4}$…$10^{-3}$ which corresponds to direct scattering by the Lunar surface.

## Introduction

The Moon has long been considered an unmagnetized body which absorbs solar wind ions as first proposed by results from the Russian missions to the Moon [*Dolginov et al.*,1966]. However, observations of the lunar plasma environment by Apollo-15 and Apollo-16 in the 1970s [*Fuller*, 1974] surprised many as a crustal magnetization was detected with surface magnetic fields up to hundreds of nanoteslas [*Dyal et al.*, 1974]. Such fields can cover regions of a few hundreds of km and are detectable at heights of up to ~100 km. Proposed theories of their origin are thermal remanent magnetization acquired during a past dynamo period (around the pre- and Nectarian period some ~4000 mln years ago), and the mechanism of amplification during large impacts [*Hood and Artemieva*, 2008].

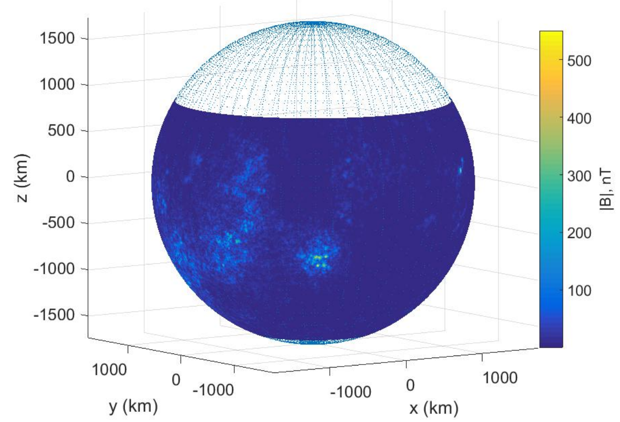


**Figure 1**. Total |B| at the surface using spherical harmonics model from [*Tsunakawa et al.*, 2015].

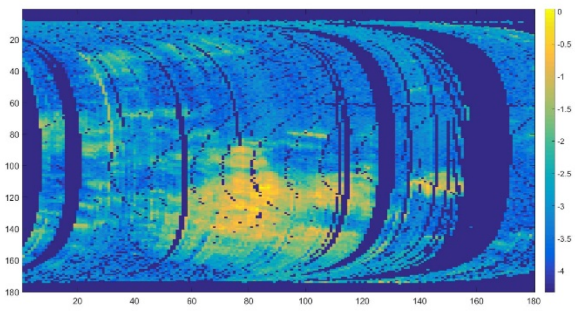

**Figure 2**. The reflection map ($\log_{10} R_i$ ). Dark blue lanes correspond to missing data.

Local magnetic structures ("Lunar Magnetic Anomalies", LMA) are highly non-dipolar and strong enough to create sub-ion scale mini-magnetospheres with characteristic sizes up to tens of kilometers [*Deca et al.*, 2014, 2018]. It has become possible recently to construct accurate Moon magnetic field models al low altitudes and at the surface based on large accumulated statistics of the magnetic field observations by such missions as Lunar Prospector (1998-1999) and Kaguya (2007-2009). In a study by [*Purucker and Nicholas*, 2010] the **B** field was reconstructed using ~ 2.7 million point observations made by Lunar Prospector magnetometer at altitudes of 11-60 km and averaged over a period of 5 s (or ~ 9 km in orbit). *Tsunakawa et al.* [2015] obtained more accurate global **B** field maps using the

Surface Vector Mapping (SVM) method based on ~5 million low altitude (10-45 km) observations made during night-side passes by the Kaguya and the Lunar Prospector spacecraft. Such detailed magnetization models are important for various aspects of lunar science, such as the study of lunar swirls (high-albedo surface markings), waves, instabilities, acceleration and deflection of solar wind plasma.

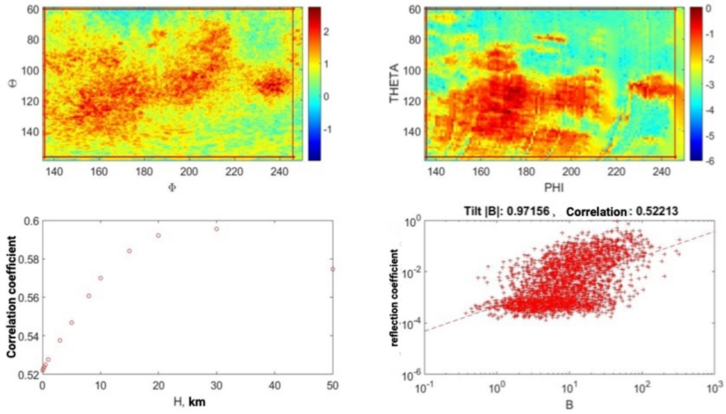


**Figure 3.** *Upper right*: $\log_{10} R_i$. *Upper left*: |B|. *Lower right*: scatterplot of Ri versus |B|. A linear regression (log-log scale) is shown dashed line. *Lower left*: Altitude dependence of the |B| - Ri correlation coefficient.

Observations of antimoonward particles are found to correlate with locations of magnetic structures on the surface. Ion sensors onboard Kaguya detected 0.1% - 1% of surface-backscattered ions [*Saito et al.*, 2008]. A more detailed study by the Chandrayaan-1 showed an increase of this value up to 10% on the strongest anomalies [*Lue et al.*, 2011] and a decrease in the ENA flux formed by the interaction of the solar wind with lunar regolith [*Vorburger et al.*, 2012; *Bhardwaj et al.,* 2015]. Charged particles are affected by the magnetic field, leading to a reduction of the ENA backscattered component over magnetic anomalies and an increase of the reflected ion component.

## Methods

In our study, we use two data sets: 1. The global spherical model of the lunar magnetic field based on Kaguya and Lunar Prospector [*Tsunakawa et al.*, 2015]. Kaguya performed observations along polar orbits at low altitudes of 9-80 km from December 2008 to June 2009 with an accuracy greater than 0.05 nT and a temporal resolution of 32 Hz. The model uses the Surface Vector Mapping (SVM) method and provides spherical coefficients $g_n^m$ and $h_n^m$ for {n,m}<450.

We calculated the magnetic field at a set of altitudes: {0, 0.1, 0.3, 0.5, 1, 3, 5, 8, 10, 15, 20, 30, 50} km. The grid of 450x900 (latitude times longitude) points corresponds to a ~12 km grid resolution, being comparable in size to some lunar swirls. Fig. 1 presents the result for h=0 km. The reconstructed field peaks at |B|~550 nT on the surface for the strongest anomalies. It is important to note that the low-altitude field is most likely underestimated because the higher harmonics (N>450) are truncated in the model.

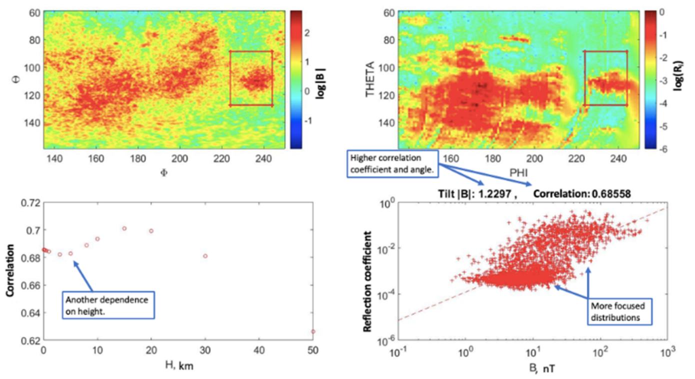


**Figure 4.** |B| - $R_i$ correlation for an isolated anomaly. Same format as Fig. 3.

The highest magnetic field intensity (718 nT) was estimated in the region antipodal to the Crisium basin, while the Imbrium and Orientale basins showed very weak (or almost nonexistent) fields, in agreement with previous studies. The magnetic field magnitude reconstructed in [*Tsunakawa et al.*, 2015] was higher than in [*Purucker and Nicholas*, 2010] due to a larger number of harmonics.

2. The solar wind ion reflection map by *Lue et al.* [2011] based on the Chandrayaan-1 data (see Fig. 2). The reflection coefficient is calculated on a grid 180˚ x 180˚ and covers the far-side hemisphere. The values are within the range $-4.5<\log_{10} R_i<0$ and the missing data are all set to 0 and are not used in our study. There are visible similarities between those two images. Despite some irregularities in the maxima positions, the reflection coefficient indeed peaks above magnetic anomalies, and also correlates well with the shape of the high |**B**| patterns, the question which we study next.

## Correlations |B| – $R_i$ : Entire area

The Pearson linear correlation coefficient and the functional dependence between $\log_{10} R_i$ and $\log_{10}$ |**B**| are investigated next taking different altitudes above the surface for the |**B**| model. First, we consider the entire domain where $R_i$ is available. |**B**| and $R_i$ are re-sampled to the same grid. Right at the surface, the |**B**|–$R_i$ correlation coefficient is 0.52.

However, the |**B**|–$R_i$ scatter plot (see, bottom right panel of Fig. 3) displays the presence of two distinct components: (1) A population for which the reflection coefficient grows with |**B**| as expected. (2) A flat population of $R_i$~$10^{-3}$ throughout the range of |**B**|'s which corresponds to surface (nonmagnetic) scattering of solar wind ions.

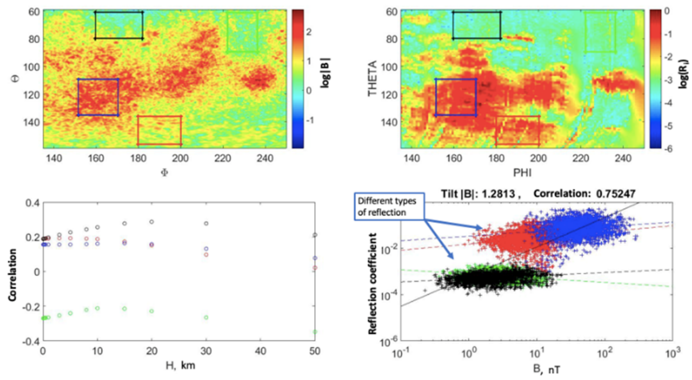


**Figure 5**. Typical areas plotted on a single Figure: anomalous and surface reflection. Same format as Fig. 3.

The functional dependence of the correlation coefficient with altitude is also considered (see bottom left panel of Fig. 3). The greatest correlation between |**B**| and $R_i$ is achieved for altitudes above 20…30 km, which we interpret as the typical vertical extent of a mini-magnetosphere. A further decrease in the correlation with height might be associated with an exponential decay of the high-N spherical harmonics and the decrease of |**B**|. Hence, magnetic anomalies get indistinguishable in the reflection coefficient at these altitudes.

## Correlations |B| – $R_i$ : An isolated anomaly area

Next let us look at an isolated anomaly. The linear correlation coefficient of the smaller region turned out to be higher than that for the entire map, but the altitude dependence is rather different (Fig. 4, left bottom panel). The altitude where the correlation coefficient peaks, is at ~15 km, which may be due to a smaller vertical scale of the anomaly than observed in other areas of the map.

The distribution of the reflection coefficient is visually similar to that of the entire map: there are two distinct components which correspond to surface reflection (constant $R_i$~$10^{-3}$) and magnetic reflection ($R_i$ ~ $|\mathbf{B}|^a$, where "a" is a power law index).

## Correlations |B| – $R_i$ : Combined picture

Next we display the magnetized and nonmagnetized regions on a single scatter plot. Fig. 5 shows correlations for high-|**B**| (marked by blue and red color) and low-|**B**| (marked by green and black color) areas. The |**B**|–$R_i$ scatter plot (Fig. 5, bottom right panel) displays several intriguing features:

(1) High-|**B**| areas have reflection coefficient which scales well with |**B**|. For weak surface magnitudes (<20 nT) a drop to ~$10^{-3}$ reflection value appears, which we interpret as a lower limit for the magnetic reflection. Indeed, taking average solar wind parameters (~400 km/s, 1 cc and proton-electron plasma), the magnetic pressure of ~20 nT is sufficient to balance the dynamic pressure. Large $R_i$ appearing for very low |**B**|<10 nT are likely a result of overlapping.

(2) Low-|**B**| areas appear for |**B**|<30 nT and have relatively narrow interval of $10^{-4}$<$R_i$ <$10^{-3}$ which is nearly independent of |**B**|. Fig. 5 (bottom right panel) shows that the linear fit makes sense only for a limited uniform patch of surface, but larger areas apparently have a nonlinear distribution of $R_i$(**B**). After some tests we found that a hyperbolic tangent function might be best describing the transition from surface to anomalous values in $R_i$(**B**) plotted in Fig. 6.

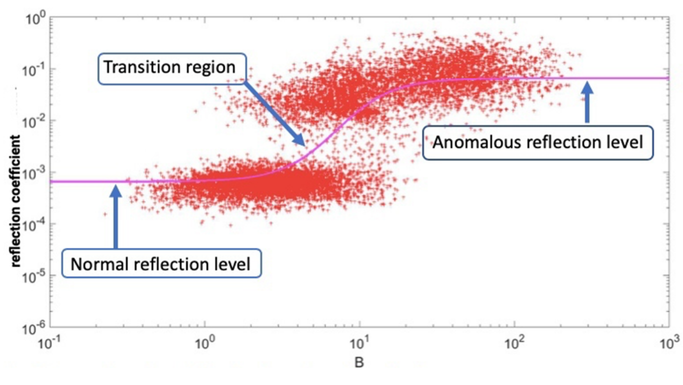


**Figure 6.** $R_i$(B) approximation: hyperbolic tangent.

## Conclusions

In this study, we investigated correlations in lunar environment data provided by two independent data sets: the model magnetic field and the reflection coefficient of incident solar wind protons. We investigated the dependence of the reflection coefficient on the magnitude of |**B**| and calculated the correlation between those two for different regions and altitudes.

The correlation peaks on average at ~20-30 km which is interpreted as average height of the lunar mini-magnetospheres.

Magnetic anomalies can efficiently reflect solar wind ions, in agreement with other observations and numerical simulations. The particle flux has a power law dependence for |**B**|>20 nT, a value which might be interpreted as a lower bound for the magnetic stand-off mechanism [*Deca et al.*, 2018]. The reflection coefficient saturates on average at $R_i$~0.1-0.3 for the largest magnetic anomalies. In the small |**B**| limit (less than 30 nT), the reflected flux ($R_i$~$10^{-3}$) is nearly independent of |**B**| since it contains particles scattered from the lunar surface and not by the magnetic anomalies. However, the presence of strong reflection $R_i > 10^{-2}$ for $|\mathbf{B}| << 20$ nT is interpreted as overlapping of $R_i$ with strong but very localized areas of magnetic shielding.

***Acknowledgements.*** Work of A.D. and I.Z. was supported by RFBR grant 19-02000993.

## References

Bhardwaj, A., Dhanya, M.B., Alok, A., Barabash, S., Wieser, M., Futaana, Y., Wurz, P., Vorburger, A., Holmström, M., Lue, C. and Harada, Y. (2015). A new view on the solar wind interaction with the Moon. Geoscience Letters, 2(1), 10.

Deca, J., and Divin, A. (2016). Reflected Charged Particle Populations around Dipolar Lunar Magnetic Anomalies. The Astrophysical Journal, 829(2), 60.

Deca, J., Divin, A., Lue, C., Ahmadi, T., and Horányi, M. (2018). Reiner Gamma albedo features reproduced by modeling solar wind standoff. Communications Physics, 1(1), 12.

Dolginov, Sh.Sh., Eroshenko, E.G., Zhuzgov, L.N., and Pushkov, N.V. (1966). Measurements of the magnetic field in the vicinity of the moon by the artificial satellite Luna 10. Dokl. Akad. Nauk SSSR, 170, 574-577.

Dyal, P., Parkin, C.W., and Daily, W.D. (1974). Magnetism and the interior of the moon. Rev. Geophys. Space Phys., 12, 568–591

Fuller, M. (1974). Lunar magnetism. Reviews of Geophysics, 12(1), 23-70. doi:10.1029/RG012i001p00023.

Hood, L., and Artemieva, N. (2008). Antipodal effects of lunar basin-forming impacts: Initial 3D simulations and comparisons with observations. Icarus, 193, 485–502.

Howard, S.K., Halekas, J.S., Farrell, W.M., McFadden, J.P., and Glassmeier, K.H. (2017). Identifying ultra low frequency waves in the lunar plasma environment using trajectory analysis and resonance conditions. Journal of Geophysical Research: Space Physics, 122(10), 9983-9993.

Lue, C., Futaana, Y., Barabash, S., Wieser, M., Holmström, M., Bhardwaj, A., Dhanya, M.B., and Wurz, P. (2011). Strong influence of lunar crustal fields on the solar wind flow. Geophysical Research Letters, 38(3).

Purucker, M.E., and Nicholas, J.B. (2010). Global spherical harmonic models of the internal magnetic field of the Moon based on sequential and coestimation approaches. Journal of Geophysical Research: Planets, 115(E12).

Saito, Y., Yokota, S., Tanaka, T., Asamura, K., Nishino, M.N., Fujimoto, M., Tsunakawa, H., Shibuya, H., Matsushima, M., Shimizu, H., and Takahashi, F. (2008). Solar wind proton reflection at the lunar surface: Low energy ion measurement by MAP-PACE onboard SELENE (KAGUYA). Geophysical Research Letters, 35(24).

Tsunakawa, H., Takahashi, F., Shimizu, H., Shibuya, H., and Matsushima, M. (2015). Surface vector mapping of magnetic anomalies over the Moon using Kaguya and Lunar Prospector observations. Journal of Geophysical Research: Planets, 120(6), 1160-1185.

Vorburger, A., Wurz, P., Barabash, S., Wieser, M., Futaana, Y., Lue, C., Holmström, M., Bhardwaj, A., Dhanya, M.B., and Asamura, K. (2012). Energetic neutral atom observations of magnetic anomalies on the lunar surface. Journal of Geophysical Research: Space Physics, 117(A7).